Response of Climate Simulation to a New Convective Parameterization in the National Center for Atmospheric Research Community Climate Model (CCM3)*

GUANG J. ZHANG

Center for Clouds, Chemistry, and Climate and Center for Atmospheric Sciences, Scripps Institution of Oceanography, La Jolla, California

JEFFREY T. KIEHL AND PHILIP J. RASCH

National Center for Atmospheric Research,+ Boulder, Colorado

(Manuscript received 1 October 1996, in final form 25 February 1997)

ABSTRACT

This study examines the response of the climate simulation by the National Center for Atmospheric Research Community Climate Model (CCM3) to the introduction of the Zhang and McFarlane convective parameterization in the model. It is shown that in the CCM3 the simulated surface climate in the tropical convective regimes, especially in the western Pacific warm pool, is markedly improved, yielding a much better agreement with the recent observations. The systematic bias in the surface evaporation, surface wind stress over the tropical Pacific Ocean in previous model simulations is significantly reduced, owing to the better simulation of the surface flow.

Experiments using identical initial and boundary conditions, but different convection schemes, are performed to isolate the role of the convection schemes and to understand the interaction between convection and the large-scale circulation in a convecting atmosphere. The comparison of the results from these experiments in the western Pacific warm pool suggests that use of the Zhang and McFarlane scheme makes a significant contribution to the improved climate simulation in CCM3. The simulated atmosphere using the Zhang and McFarlane scheme exhibits a quasi-equilibrium between convection and the large-scale processes. When this scheme is removed from the CCM3, such a quasi-equilibrium is no longer observed. In addition, the simulated thermodynamic structures, the surface evaporation, and surface winds in the Pacific warm pool become very similar to those in the CCM2 climate.

Examination of the temporal evolution of the various fields demonstrates that the stabilization of the atmosphere using the new convection scheme takes place during the transition from nonequilibrium to quasi equilibrium at the beginning of the time integration. After quasi equilibrium is reached, the atmosphere is warmer and more stable compared to the run without the new scheme. Associated with the more stable stratification, the atmospheric circulation becomes weaker, thus the surface winds and evaporation are weaker because of the coupling between thermodynamics and dynamics in the tropical troposphere.

1. Introduction

The Community Climate Model (CCM) of the National Center for Atmospheric Research has been widely used for global climate studies. The previous model version (CCM2) is able to simulate many of the observed climate features and the earth's radiation budget (Hack et al. 1994; Kiehl 1994; Kiehl and Briegleb 1992; Kiehl et al. 1994). These include the intertropical convergence zone (ITCZ) and the monsoonal regimes in the Tropics, outgoing longwave radiation, planetary albedo, and shortwave and longwave cloud radiative forcing. Nevertheless, there are several important deficiencies in the model simulation of precipitation and surface climatology that have serious implications for any atmosphere–ocean model coupling effort. The simulated precipitation maximum, ocean surface evaporation, and wind stress are excessively high in comparison to the observations. Furthermore, the simulated precipitation tends to unrealistically concentrate over certain areas and to be locked over some orographic features in southeast Asia and off the west coast of Central America, creating excessive precipitation maxima in various tropical locations.

The simulated surface evaporation over the tropical oceans, particularly the western Pacific warm pool, is, in general, too large (Kiehl et al. 1995; Zhang 1996).

* Report 169 of the Center for Clouds, Chemistry, and Climate (C4).

+ The National Center for Atmospheric Research is sponsored by the National Science Foundation.

Corresponding author address: Dr. Guang J. Zhang, Center for Clouds, Chemistry, and Climate, Scripps Institution of Oceanography, La Jolla, CA 92093-0221.
E-mail: gzhang@ucsd.edu

While the observed surface evaporation in the warm pool is on the order of 100 W m^{-2} (Oberhuber 1988; Zhang and McPhaden 1995; Ramanathan et al. 1995), the evaporation simulated by CCM2 is close to 160 W m^{-2}. This excessively high evaporation is attributed to the strong hydrological cycle and the associated strong surface winds in the CCM2 climate (Zhang 1996).

Extensive effort has been devoted to improving the CCM2 climate model. This includes the changes in radiative parameterization, representation of the atmospheric boundary layer, and convective parameterization. While the changes in radiative parameterization and boundary layer parameterization have reduced the systematic bias in the surface and top of the atmosphere radiation budget, and have improved the estimates of boundary layer height, the implementation of a new convective parameterization scheme developed by Zhang and McFarlane (1995) has further improved the simulation of precipitation, surface evaporation, and surface wind stress. Motivated by this improvement in the CCM3 climate simulation, the present study attempts to investigate the role of convection as represented by the Zhang and McFarlane (1995) scheme (hereafter referred to as ZM scheme) in CCM3. We will mainly focus on the dynamic and thermodynamic aspects of the model response to the new convection scheme.

The organization of the paper is as follows. Section 2 describes the experiment design for this study. Section 3 briefly outlines the ZM convective parameterization scheme. In section 4, the changes of the climate simulation in CCM3 from the previous model version are described by simulating the surface climate and the atmospheric thermodynamic structures, both of which are very sensitive to convective parameterization. The mechanism through which convection influences the climate simulation is examined to section 5, where the interaction mechanism between convection and the large-scale circulation in CCM3 is discussed through comparisons of three 150-day simulations. Some concluding remarks are presented in section 6.

2. Experiment design

For this study, we use the data from two long-term simulations, both of which use the observed time-varying sea surface temperature (SST) from the Atmospheric Model Intercomparison Project (AMIP) as surface boundary conditions (Gates 1992). The first simulation (referred to as CCM2) is one of the AMIP simulations using CCM2 as documented by Hack et al. (1993). Moist convection is parameterized using the scheme developed by Hack (1994). The simulation starts on 1 September 1984 with the initial conditions from a previous model simulation and runs for five years. The second simulation is from the standard CCM3 (referred to as CCM3). It also uses the AMIP SST for boundary conditions. A major difference from the first simulation is the incorporation of the ZM scheme, in conjunction with the Hack (1994) scheme. The other differences are the improved representation of radiative transfer processes, boundary layer processes, and the inclusion of a land surface model of Bonan (1996) in CCM3. Changes to the representation of radiative transfer include the incorporation of minor CO_2 bands trace gases in the longwave and a background aerosol in the shortwave. Improvements are also made in the diagnostics of cloud optical properties and the incorporation of the radiative properties of ice clouds. The boundary layer parameterization has been revised to yield better estimates of boundary layer height. Kiehl et al. (1996) and Kiehl et al. (1998a) give a detailed description of CCM3. The model and observational results to be presented in section 4 are averaged over five Julys from 1985 to 1989, unless otherwise stated.

The ZM scheme is designed primarily for deep penetrative convection. Although shallow convection is also allowed, the scheme does not produce enough of it because shallow convection is considered only when no deep convection is generated by the scheme at a time step. In the presence of strong trade inversion, the scheme should be able to produce shallow convection. When used alone, due to the efficient transport of moisture out of the boundary layer to the upper troposphere, the scheme results in a lower troposphere drier than observed. This would affect the low-level cloud distribution, which in turn would affect the surface radiation budget. Inclusion of a shallow convection parameterization helps to moisten the lower troposphere. For this purpose, the Hack scheme is used to parameterize shallow convection. Thus, in the CCM3 model configuration, the ZM scheme is activated first to generate deep convection, followed by the Hack scheme to represent shallow and possible midlevel convection. For this study, we take five years of the model output from 1985 to 1989 for both the CCM2 and CCM3 simulations and use average July results over these years to demonstrate the improvement of the model simulations in CCM3.

Because of the modifications in the representation of the many processes from CCM2 to CCM3, the improvement in CCM3 simulation cannot be unequivocally attributed to the addition of the improved representation of a particular physical process in the model. To isolate and understand the role of the new convection scheme in the improvement of the model simulation, two short runs (150 days) are performed. The first one (referred to as ZMH) uses the standard CCM3 model, but with the initial conditions used for the 5-yr CCM2 run—that is, 1 September 1984. The same analyzed AMIP SST dataset as in the long runs is used for the boundary conditions. The second 150-day run (referred to as NOZM) is identical to ZMH in every aspect, including initial and boundary conditions, except the ZM convection scheme is removed from the model. The time series from CCM2 for the same 150 days will also be used. Thus, in effect there are three 150-day simulations. Table 1 summarizes these experiments. The underlying

TABLE 1. List of the 150-day-long experiments using CCM2 and CCM3 models.

Experiment name	Model used	Initial conditions	Boundary conditions	Convection scheme
ZMH	CCM3	1 Sep 1984 from previous CCM2 model output	AMIP SST	ZM + Hack
NOZM	CCM3	Same	Same	Hack
CCM2	CCM2	Same	Same	Hack

logic for designing such experiments is that because every aspect of the ZMH and NOZM experiments is identical except the convection scheme, the difference between ZMH and NOZM would underline the effect of the ZM scheme. On the other hand, both the CCM2 and NOZM experiments use the Hack scheme for convection, but the NOZM configuration contains all the modifications from CCM2 to CCM3 other than the convective parameterization (e.g., radiation parameterization, boundary layer parameterization, land surface parameterization, change of model tunable parameters, change of model numerics, etc.). Thus, the difference between these two experiments would signify the effect of the changes other than the convective parameterization that would contribute to the improvement from CCM2 to CCM3. Through the analyses of these short runs, we attempt to understand how convection interacts with the large-scale fields and contributes to the improved simulation in CCM3.

3. The Zhang–McFarlane scheme

This section will outline the ZM convection scheme. For details, the reader is referred to Zhang and McFarlane (1995). The scheme is based on a plume ensemble approach where it is assumed that an ensemble of convective-scale updrafts and their associated downdrafts may exist when the atmosphere is conditionally unstable in the lower troposphere. The updraft ensemble comprised of plumes rooted in the planetary boundary layer can penetrate into the upper troposphere until their neutral buoyancy levels. Convection occurs only when there is convective available potential energy (CAPE), which is subsequently removed by convection at an exponential rate using a specified adjustment timescale.

The large-scale effect of convection on the temperature and moisture fields in the cloud layer and subcloud layer are given in the following. In the cloud layer it is represented by

$$C_p\left(\frac{\partial T}{\partial t}\right)_{cu} = -\frac{1}{\rho}\frac{\partial}{\partial z}(M_u S_u + M_d S_d - M_c S) + L(C - E) \tag{1}$$

and

$$\left(\frac{\partial q}{\partial t}\right)_{cu} = -\frac{1}{\rho}\frac{\partial}{\partial z}(M_u q_u + M_d q_d - M_c q) - (C - E); \tag{2}$$

in the subcloud layer it can be written as

$$C_p\left(\frac{\partial T}{\partial t}\right)_m = -\frac{1}{\Delta z_m}\{M_b[S(z_m) - S_u(z_m)] + M_d(z_m)[S(z_m) - S_d(z_m)]\} \tag{3}$$

and

$$\left(\frac{\partial q}{\partial t}\right)_m = -\frac{1}{\Delta z_m}\{M_b[q(z_m) - q_u(z_m)] + M_d(z_m)[q(z_m) - q_d(z_m)]\}, \tag{4}$$

where the net vertical cloud mass flux M_c is composed of updraft mass flux M_u and downdraft mass flux M_d; C and E are the large-scale mean rates of condensation and evaporation, respectively; and S, S_u, S_d, q, q_u, and q_d are the corresponding values of the dry static energy and specific humidity for the large-scale, the updraft ensemble, and the downdraft ensemble, respectively. Here Δz_m is the depth of the subcloud layer, the subscript "m" denotes the subcloud layer properties, z_m is the height of the subcloud layer, and M_b is the cloud base mass flux for the updraft ensemble.

A cloud model is used to determine the mass flux and the thermodynamic properties in the updraft and downdraft ensembles. The updraft ensemble is represented as a collection of entraining plumes, each with a characteristic fractional entrainment rate. Mass carried upward by a plume is detrained into the environment in a thin layer at the top of the plume, where the detrained air is assumed to have the same temperature as in the environment and to be saturated. The top of the shallowest of the convective plumes is assumed to be no lower than the height of the minimum in saturated moist static energy h^* (typically in the midtroposphere), ensuring that the cloud-top detrainment is confined to the conditionally stable layer of the atmospheric column. Each plume is assumed to have the same value for the cloud base mass flux, giving the vertical distribution of the cloud mass flux for the updraft ensemble as

$$M_u = M_b \int_0^{\lambda_D} \frac{1}{\lambda_0} e^{\lambda(z - z_m)}\, d\lambda, \tag{5}$$

where λ_0 is the maximum entrainment corresponding to the shallowest of the updraft plume ensemble, and λ_D is the entrainment rate for the updraft that detrains at height z and is determined by the following integral equation:

$$h(z_m) - h^* = \lambda_D \int_{z_m}^{z} [h(z_m) - h(z')]e^{[\lambda_D(z'-z)]}\, dz'. \quad (6)$$

Given the ensemble updraft mass flux, the budget equations for dry static energy, specific humidity, and cloud water l, are written as

$$\frac{\partial}{\partial z}(M_u S_u) = (E_u - D_u)S + LC_u, \quad (7)$$

$$\frac{\partial}{\partial z}(M_u q_u) = E_u q - D_u q^* - C_u, \quad \text{and} \quad (8)$$

$$\frac{\partial}{\partial z}(M_u l) = -D_u l + C_u - R_r, \quad (9)$$

where the conversion from cloud water to rainwater is given by

$$R_r = C_0 M_u l, \quad (10)$$

with $C_0 = 2 \times 10^{-3}\ \text{m}^{-1}$.

In the ZM scheme, each precipitating updraft has a corresponding downdraft that is initiated from the bottom of the updraft detrainment layer. Detrainment of downdraft is confined to the subcloud layer. Accordingly, the ensemble downdraft mass flux takes a similar form to (5), the initial downdraft mass flux being a fraction of the updraft mass flux to ensure that the net vertical mass flux at the cloud base is upward.

The parameterization is closed by relating the cloud base mass flux to the consumption rate of CAPE generated by the large-scale processes. Since the large-scale temperature and moisture changes in both the cloud layer and the subcloud layer due to convective activity are linearly related to the cloud base mass flux—for example, Eq. (1) to Eq. (4)—the CAPE change due to convection can be written as

$$\left(\frac{\partial \text{CAPE}}{\partial t}\right)_{cu} = -M_b F, \quad (11)$$

where F is the CAPE consumption rate by convection per unit cloud base updraft mass flux and is determined by the large-scale thermodynamic profiles and the cloud model. The closure condition is that the CAPE is removed at an exponential rate by convection with a characteristic adjustment timescale τ. Thus

$$M_b = \frac{\text{CAPE}}{\tau F}, \quad (12)$$

where τ is typically a few hours.

The Hack scheme is considerably different from the deep convection scheme. It assumes that clouds consist of successive plumes occupying three model layers in depth, with the first plume starting from the top of the boundary layer and the next one starting one layer above, and so on. Each plume carries a certain amount of cloud mass from its base height and detrains a fraction in the model layer immediately above. The rest is detrained in the third layer from the plume base. The amount of the cloud base mass flux at each plume base is determined by the local atmospheric instability. The only connection between plumes starting at the lower levels and those starting at the upper levels is through the modification of the environmental air by the lower-level plumes. Therefore, this scheme is in many ways similar to moist convective adjustment, except the adjustment is expressed explicitly in the mass flux form and is performed in three layers successively from bottom to top at each time step.

4. Model response

The changes of the climate simulation from CCM2 to CCM3 will be described in this section by comparing the surface climate and the thermodynamic structures from the CCM2 and CCM3 simulations. The examination of how convection affects the large-scale fields to result in the simulated climate will be deferred to the next section. We will mostly focus on the simulation difference in the Tropics, where convection is the most active and thus has the most pronounced effects on the atmospheric dynamic and thermodynamic fields. For a more thorough documentation of the CCM3 climate and its seasonal variation, see Kiehl et al. (1998a), Kiehl et al. (1998b), Hack et al. (1998), and Hurrell et al. (1998).

a. Surface climate

Figure 1 shows the distribution of precipitation from CCM2, CCM3, and the observations from the Global Precipitation Climatology Project (GPCP) for five Julys from 1985 to 1989. Although the CCM2 is able to simulate the major precipitation centers, such as the ITCZ in the Pacific and the southeast Asian and Central American monsoon systems, there are unrealistically high, localized precipitation maxima in the South China Sea, the western Pacific warm pool, and Central America compared to the observations. The precipitation zone in the central and western tropical Pacific is about 5°–10° too far north. The CCM3 simulation, on the other hand, produces a much better geographical distribution of precipitation, particularly a more realistic simulation of the Indian monsoon and the maximum precipitation off the west coast of Central America, although the heavy precipitation region in Central America seems to extend too far into the Caribbean Sea. The magnitude of the precipitation in the western Pacific and the Indian monsoon is comparable to the GPCP observations. The overall precipitation distribution is much smoother and less localized than the CCM2 run. Although there are uncertainties among different precipitation datasets, for example, GPCP versus Legates and Willmott (1990), the improvement from CCM2 to CCM3 is apparently beyond the observational uncertainties.

Excessive surface evaporation in CCM2 over the tropical Pacific has been noted when compared to the

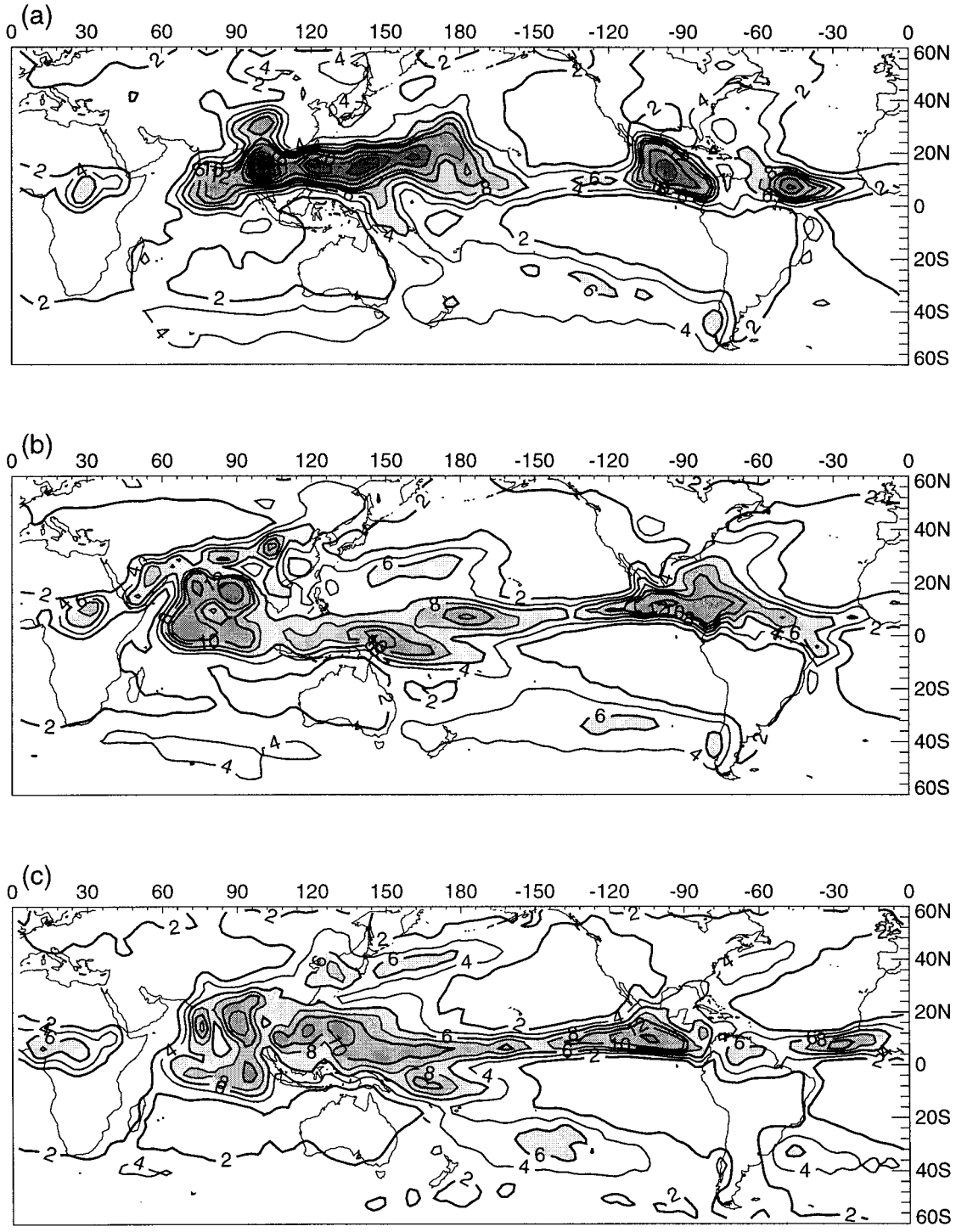

FIG. 1. Global distribution (60°N–60°S) of precipitation for July from (a) CCM2 simulation, (b) CCM3 simulation, and (c) GPCP satellite retrieval. Contour intervals are 2 mm day^{-1} at 12 mm day^{-1} and below, and 4 mm day^{-1} above. Contours greater than 6 mm day^{-1} are shaded.

observations (Kiehl et al. 1995; Zhang 1996). It was one of the major problems that hindered the coupling between CCM2 and the ocean models for climate studies. In CCM3, this problem is significantly alleviated. Figure 2 shows the global distribution of surface evaporation from CCM2, CCM3, and their difference. A distinct feature in the simulated surface evaporation from CCM3 is a relatively low evaporation zone in the equatorial Pacific. This contributes to the well-simulated minimum evaporation in the zonal mean (Kiehl et al. 1998b) compared to the observations. In the western Pacific warm pool, the magnitude of evaporation (near 100 W m^{-2}) is close to the climatology from the Coupled Ocean–Atmosphere Data Sets (COADS, Oberhuber 1988) and the more recent observations from the moored buoys and the Central Equatorial Pacific Experiment field experiment (Zhang and McPhaden 1995; Ramanathan et al. 1995; Zhang and Grossman 1996). On the other hand, the CCM2 simulation fails to produce a clear minimum in the equatorial Pacific. Furthermore, evaporation over the warm pool is significantly higher, by about 50%. Table 2 shows the average evaporation over the equatorial western Pacific (140°–170 E, 8°S–8°N), central Pacific (170°E–150°W, 8°S–8°N), and eastern Pacific (150°–110°W, 8°S–8°N) from CCM2, CCM3, and the observations from the tropical atmosphere–ocean (TAO) buoys deployed in the equatorial Pacific. The evaporation estimates from the buoys are obtained by applying a bulk parameterization (Zhang and McPhaden 1995) to the hourly buoy data for five-and-a-half years (January 1991 to July 1996). In both the western and central equatorial Pacific, the evaporation from CCM3 is much closer to the observed values than that from CCM2. In the eastern equatorial Pacific, evaporation values from both CCM2 and CCM3 are high compared to the observations, with CCM3 giving a slightly better simulation. The difference between CCM3 and CCM2 (Fig. 2c) shows that surface evaporation in CCM3 is significantly reduced in major precipitation regimes, such as the Central American monsoon, Indian Ocean, and the western Pacific warm pool, by 50 W m^{-2} or more. Reduction of similar magnitude in evaporation for January in the central and western tropical Pacific is also observed (not shown) from CCM2 to CCM3. However, in the subtropical trade wind regions, the surface evaporation in CCM3 is higher than that in CCM2, and it is also higher than the observed values (Kiehl et al. 1998b). This is due to the stronger trade winds associated with the stronger subtropical surface high pressure centers compared to the observations (Hurrell et al. 1998).

Another serious deficiency of the simulated surface climatology by CCM2 is the excessive surface wind stress over the tropical Pacific (Hurrell et al. 1993). If coupled with an ocean circulation model, it would provide an unrealistic dynamic driving force to the ocean circulation. In CCM3, this deficiency is largely removed. Figure 3 shows the zonal and meridional wind stress across the equatorial Pacific [averaged within (8°S, 8°N)] from the CCM2, CCM3, the European Centre for Medium-Range Weather Forecasts (ECMWF) analysis, the Florida State University (FSU) dataset, and the TAO buoy data. The buoy values are based on the same five-and-a-half-year hourly buoy observations as in the estimates of the surface evaporation and the bulk formula by Zhang and McPhaden (1995). Using the bulk formula, the hourly zonal and meridional wind stress is computed. The monthly mean wind stress values are obtained by first averaging the hourly values to get the daily mean and then further averaging the daily means to get the monthly mean wind stress. All July wind stress values from each buoy are averaged to obtain the July climatology. The surface wind stress data from The Florida State University (FSU) are based on the COADS dataset for the month of July from 1985 to 1989.

The largest easterly wind stress is observed in the eastern Pacific near 140°W, decreasing westward to become very weak in the western Pacific. The buoy observed zonal wind stress is stronger in the eastern Pacific but slightly weaker toward the western end of the warm pool in comparison to the FSU wind stress. Two factors may contribute to this difference. First, the buoy observations cover the period from 1991 to 1996, whereas the FSU data cover the period from 1985 to 1989. The early 1990s are dominated by the El Niño conditions, giving stronger than normal zonal wind stress in the east and weaker than normal zonal wind stress in the west (M. McPhaden 1997, personal communications). Second, the FSU wind stress is based on the COADS dataset, which may have large uncertainties compared to the buoy data. The ECMWF analyzed wind stress is reasonably close to the buoy observations west of 160°W but is significantly less than the buoy values in the eastern equatorial Pacific. It is also less than the FSU observations. Underestimation of the easterly wind stress in the eastern equatorial Pacific in the National Centers for Environmental Prediction reanalysis is also noticed by Smull and McPhaden (1996). On the other hand, the zonal wind stress in the CCM3 simulation is reasonably close to both the buoy and FSU observations across the equatorial Pacific, except west of 160°E, where the large easterly wind stress is due to the stronger than observed southeasterly wind northeast off Australia and east of Papua New Guinea. In comparison, the easterly wind stress from the CCM2 simulation is too strong in the entire central and western equatorial Pacific and comparable to that from CCM3 in the eastern equatorial Pacific.

The basinwide variation and magnitude of the buoy-observed meridional wind stress is very well captured in the ECMWF analysis. The FSU meridional wind stress is somewhat higher than the buoy values across the equatorial Pacific. Compared to the observations, the meridional wind stress from the CCM2 simulation is systematically more southerly across the equatorial Pacific. On the other hand, CCM3 produces a signifi-

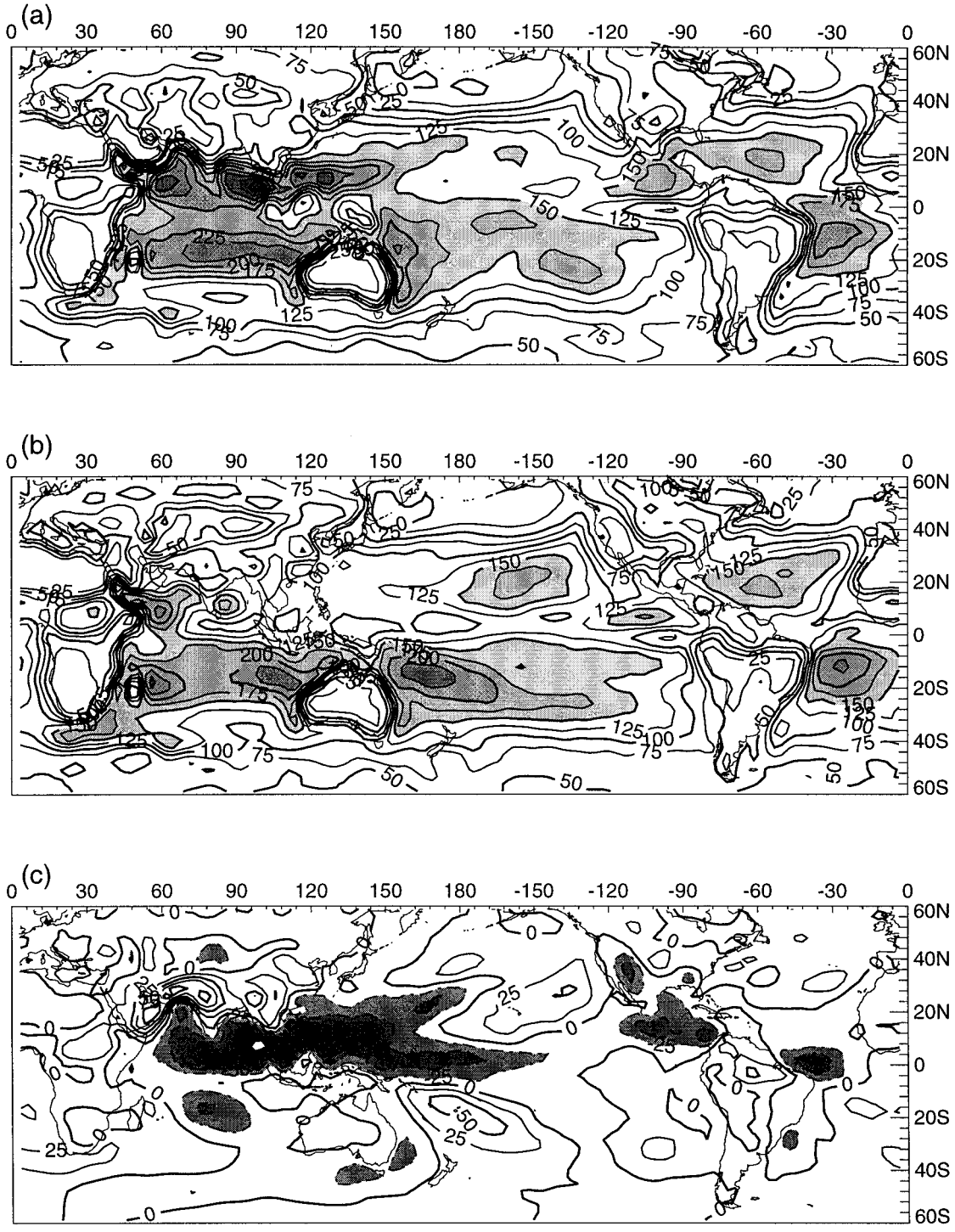

FIG. 2. Global distribution of surface latent heat flux for July from (a) CCM2 simulation, (b) CCM3 simulation, and (c) their difference (CCM3 − CCM2). Contour intervals are every 25 W m^{-2}. Contours greater than 150 W m^{-2} are shaded in (a) and (b), and contours less than −25 W m^{-2} are shaded in (c).

TABLE 2. Surface evaporation in the equatorial Pacific from model simulations and long-term buoy observations (W m^{-2}).

	Western Pacific (140–170°E) and (8°S–8°N)	Central Pacific (170°E–150°W) and (8°S–8°N)	Eastern Pacific (150–110°W) and (8°S–8°N)
CCM2	156	158	138
CCM3	119	129	131
Buoys	107	119	101

cantly better meridional wind stress simulation almost everywhere across the equatorial Pacific except the far eastern Pacific, where both the CCM2 and CCM3 have too strong a southerly wind stress. The simulation of the surface wind stress in other regions of the world oceans is described in Hurrell et al. (1998). There is a significant improvement in the simulated surface wind stress in the Arabian Sean, the Bay of Bengal, and the subtropical Pacific off the southeast Asian maritime landmass due to the improvement of the low-level southwesterly flow in association with the Indian monsoon and the western Pacific convection. However, same as in the surface evaporation, the easterly and equatorward wind stress in the trade wind regions is somewhat too strong because of the stronger than observed trade winds in CCM3.

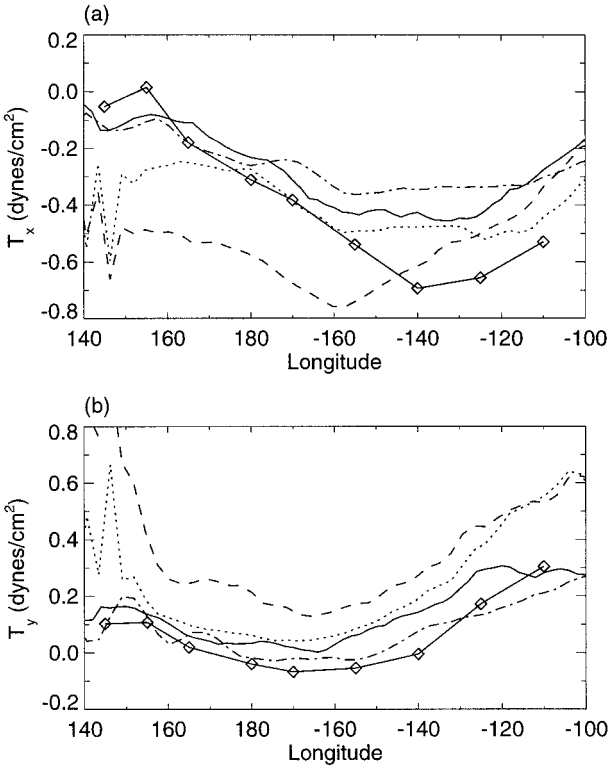

FIG. 3. Distribution of the surface (a) zonal and (b) meridional wind stress across the equatorial Pacific (averaged from 8°S to 8°N) from the buoy observation (solid line with diamond nodes), FSU COADS observations (solid line), ECMWF analysis (dashed–dotted line), CCM2 (dashed line), and CCM3 (dotted line).

b. Thermodynamic structure

The thermodynamic structure of the atmosphere is significantly affected by the changes in the model physical parameterization. The simulated thermodynamic structure in CCM3 is described in Hack et al. (1998). To summarize, while the overall observed thermal structures are well simulated in CCM3, there are some systematic biases. The tropical troposphere exhibits a weak warm bias in CCM3 compared to a cold bias in CCM2. An upper-tropospheric cold bias above 200 mb becomes more pronounced in CCM3 than in CCM2. Some high-latitude cold biases that appeared in CCM2 also remain in CCM3. To demonstrate the effect of the deep convection parameterization and its possible contribution to some of the biases in the Tropics, we will compare the simulated thermodynamic structure with the climatology from the soundings at Truk Island (151°E, 7.5°N) in the western Pacific. Figure 4 shows the profiles of temperature, specific humidity, and the equivalent potential temperature from CCM2, CCM3, and the observations for July. Also shown are the temperature and moisture differences from the observations and the buoyancy profiles of the parcels lifted reversible moist adiabatically from the lowest model level. The profiles from the model simulations are obtained from the nearest four grid points surrounding the island. While there is a clear and very significant improvement in precipitation, surface evaporation, and surface wind stress over the western Pacific in CCM3 as shown earlier, the comparison of the thermodynamic structures between CCM2, CCM3, and the soundings shows some apparent general weakness of the CCM3 thermodynamic structures. There is an excellent agreement in temperature between CCM3 and the observations from the surface up to the 800-mb level. In the mid- to upper troposphere from 700 to 200 mb, the CCM3 temperature is warmer by 1°–1.5°C. On the other hand, the CCM2 temperature is warmer than the observations by 1°–2°C from the surface to 800 mb. In the mid- to upper troposphere from 700 to 200 mb, the CCM2 temperature has a much better agreement with the observations, warmer than the observations by less than 0.5°C. From 200 mb to the tropopause, both the CCM2 and CCM3 temperatures have a relatively large cold bias, a general feature as mentioned above. An inspection of the horizontal distribution of the temperature at the 138-mb model level and the top of the atmosphere longwave and shortwave radiative fluxes (not shown) indicates that the CCM3 temperature is systematically lower than the CCM2 temperature everywhere in the latitude belt from 20°S to 20°N, and this change is not correlated to the changes in the radiative fluxes in spatial distribution. Recent sensitivity experiments by Williamson et al. (1998) indicate that this cold bias compared to the observations is ba-

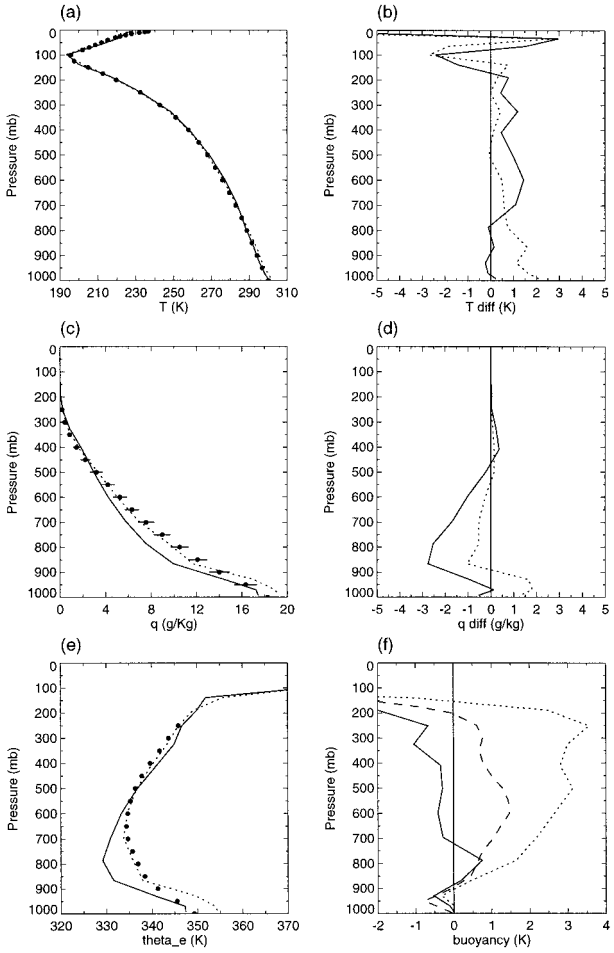

FIG. 4. Vertical profiles of (a) temperature, (b) temperature difference from the observations, (c) specific humidity, (d) specific humidity difference from the observations, (e) equivalent potential temperature, and (f) buoyancy for July at Truk Island in the western Pacific warm pool from CCM2 (dashed line) and CCM3 (solid line). The observations [black dots in (a), (c), and (e), and dashed line in (f)] are from the soundings at Truk Island. The standard deviations from the observations are shown as error bars.

sically due to numerical errors caused by insufficient vertical resolution and that going to more layers largely solves this problem. Other changes, such as using Lagrangian dynamic transport or modifying the cloud microphysical properties, which are important to the radiative heating, can also improve the simulation.

The moisture profile in CCM2 shows much better agreement with the observations than that in CCM3 from 900 mb up. The atmosphere in CCM3 is much drier than observed from 950 to 450 mb, by as much as 2–3 g kg^{-1} in the lower troposphere above the boundary layer, and too moist from 400 mb upward. However, in the boundary layer CCM3 moisture is in excellent agreement with the observations. The dry bias in the lower troposphere is a broad unwanted feature in CCM3 and it appears in other locations and seasons as well (Hack et al. 1998). Since water vapor is the most important greenhouse gas in the atmosphere, its vertical distribution strongly affects the atmospheric radiation. Thus, the relatively poor simulation of the moisture field in CCM3 could have some significant implications for climate studies with the model. An effort is currently under way to improve this aspect of the model (see discussions below). The moisture simulation in CCM2 is significantly better than in CCM3 in the free troposphere. However, it is much too moist in the boundary layer below 900 mb, by more than 1.5 g kg^{-1}. This moist bias, together with the large warm bias near the surface, results in a large error in equivalent potential temperature, about 5 K, in CCM2 near the surface compared to the observations. Above the boundary layer, the errors of the opposite sign in temperature and moisture in CCM2 largely offset each other to give an equivalent potential temperature profile in very good agreement with the observations. On the other hand, due to the dominant contribution from the moisture errors in CCM3, the equivalent potential temperature in the lower to middle troposphere is significantly lower than the observations. However, in the boundary layer, the agreement between the CCM3 equivalent potential temperature and the observed values is excellent.

The dry bias in the lower troposphere and moist bias in the middle to upper troposphere in CCM3 seem to be largely related to the introduction of the ZM scheme. Persistent convection resulting from the unrealistic interaction with the planetary boundary layer (PBL) dries the lower troposphere and moistens the mid- to upper troposphere through detrainment of the cloud water and moist air. It may also be responsible for failure to simulate the Madden–Julian oscillation in CCM3 as recently diagnosed (D. Randall 1997, personal communication). Experiments with the CCM3 model and the ZM scheme by P. Rasch and J. Petch (1997, personal communication) suggest that the moisture simulation in the lower troposphere can be significantly improved by including a trigger function (which prevents convection in situations where parcels originating near the surface encounter a region of strong negative buoyancy) and modifying the interaction between convection and the PBL parameterization. These revisions result in a substantially moister lower troposphere. The addition of the trigger function also changes the temporal aspects of convection in the model, and this influences model behavior on many timescales, varying from the diurnal to the seasonal. The details of these results will be presented elsewhere.

Despite the relatively poor thermodynamic structure in the free troposphere, the simulated CAPE in CCM3 is closer to the observed value. The CAPE values using the CCM2 and CCM3 temperature and moisture profiles are 1300 and 20 J kg^{-1}, respectively, assuming the air parcels at the lowest model level are lifted reversible moist adiabatically to their respective neutral buoyancy levels. The CAPE value from the observed soundings is about 300 J kg^{-1}, assuming the air nearest the lowest

model level is lifted. Noting that CAPE is the vertical integral of the buoyancy of the air parcels lifted from the surface, we also show in Fig. 4 the buoyancy profiles for CCM2, CCM3, and the observations. The CCM3 buoyancy profile is slightly negative at most of the levels. The buoyancy from the observations is about 1°–1.5°C up to the 200-mb level. This profile is very similar to the buoyancy profile in Xu and Emanuel (1989), who used the sounding data from 1 July to 30 September 1965–80 at Truk Island to estimate the degree of instability in the tropical atmosphere. Considering that the uncertainty or instrumental errors in their buoyancy calculations is about 1°C, they concluded that the tropical atmosphere is neutrally stable. This suggests that the simulated tropical atmosphere in CCM3 is also neutrally stable. On the other hand, the buoyancy in CCM2 is much larger, more than 2°C in most of the troposphere. The difference in buoyancy between CCM2 and the observations is apparently largely due to the warmer and more moist boundary layer air in CCM2 because the thermodynamic structures in the free troposphere are very similar. This illustrates the fact that CAPE is determined by many factors, including the tropospheric thermal structure and the boundary layer temperature and moisture, and the same CAPE value can come from very different thermodynamic profiles, and vice versa. Since the tropical circulation is highly dependent on the atmospheric stability (Neelin and Held 1987; Zhang 1994), this may explain the weaker and better simulation of the tropical circulation in CCM3.

The top of the atmosphere radiation budget is an important parameter of the climate system and is affected by the simulation of convection, clouds, the temperature, and moisture distribution. Figure 5 shows the zonal averages of the longwave, shortwave, and net radiative fluxes as well as the cloud radiative forcing at the top of the atmosphere for the five July averages. In general, most of the changes come from the cloud radiative forcing. The increase in the longwave cloud forcing at 10°N and the decrease in the Southern Hemisphere midlatitudes from CCM2 to CCM3 generally improves the agreement with the Earth Radiation Budget Experiment observations; so does the reduction in shortwave cloud forcing in the Tropics. For the details of the CCM3 radiation budgets, see Kiehl et al. (1998b).

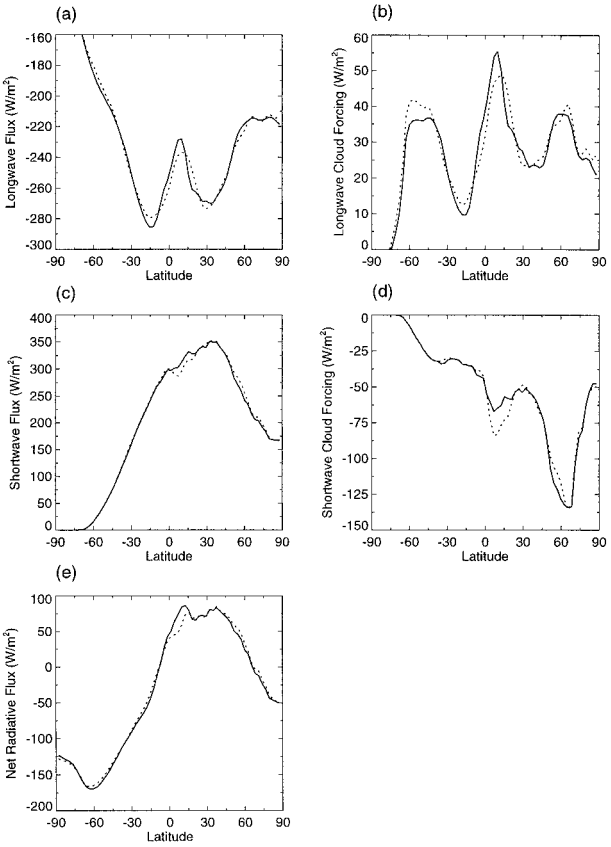

FIG. 5. The zonal averages of the (a) longwave radiative flux, (b) longwave cloud forcing, (c) shortwave radiative flux, (d) shortwave cloud forcing, and (e) net radiative flux at the top of the atmosphere for the five July averages of CCM3 (solid) and CCM2 (dashed).

5. Interaction of convection with the large-scale circulation

As mentioned in section 2, there are many changes from CCM2 to CCM3, including the parameterization of the radiative transfer, boundary layer processes, and deep convection. In this section we will examine the contribution from the introduction of the ZM convection scheme to the changes in the simulated climate using the results in the western Pacific warm pool from three 150-day runs. We will also examine the mechanism of the interaction of convection with the large-scale dynamics and thermodynamics through which convection realizes its role in the climate simulation. As described in detail in section 2, the first experiment (ZMH) uses the CCM3 configuration but with the initial conditions for the CCM2 to start the integration. The second experiment (NOZM) is identical to the first one except without the ZM scheme. The third simulation is taken from the first 150 days of the 5-yr CCM2 simulation presented in section 4. It covers the same time period as the other two experiments. All the runs start from the same initial conditions on 1 September 1984, with the analyzed AMIP SST for boundary conditions. The western Pacific warm pool is one of the most active convective regions; thus, it is ideal for examining the interaction between convection and the large-scale circulation. In the rest of this study, the warm pool region is defined as an area bounded by (140°E, 170°E) and (10°S, 10°N). All the profiles and time series shown below are averaged over this area, unless otherwise stated.

Convective heating and drying measure the response of convection to the large-scale forcing. One major difference between the ZM scheme and the Hack scheme is that the ZM scheme represents convection by deep

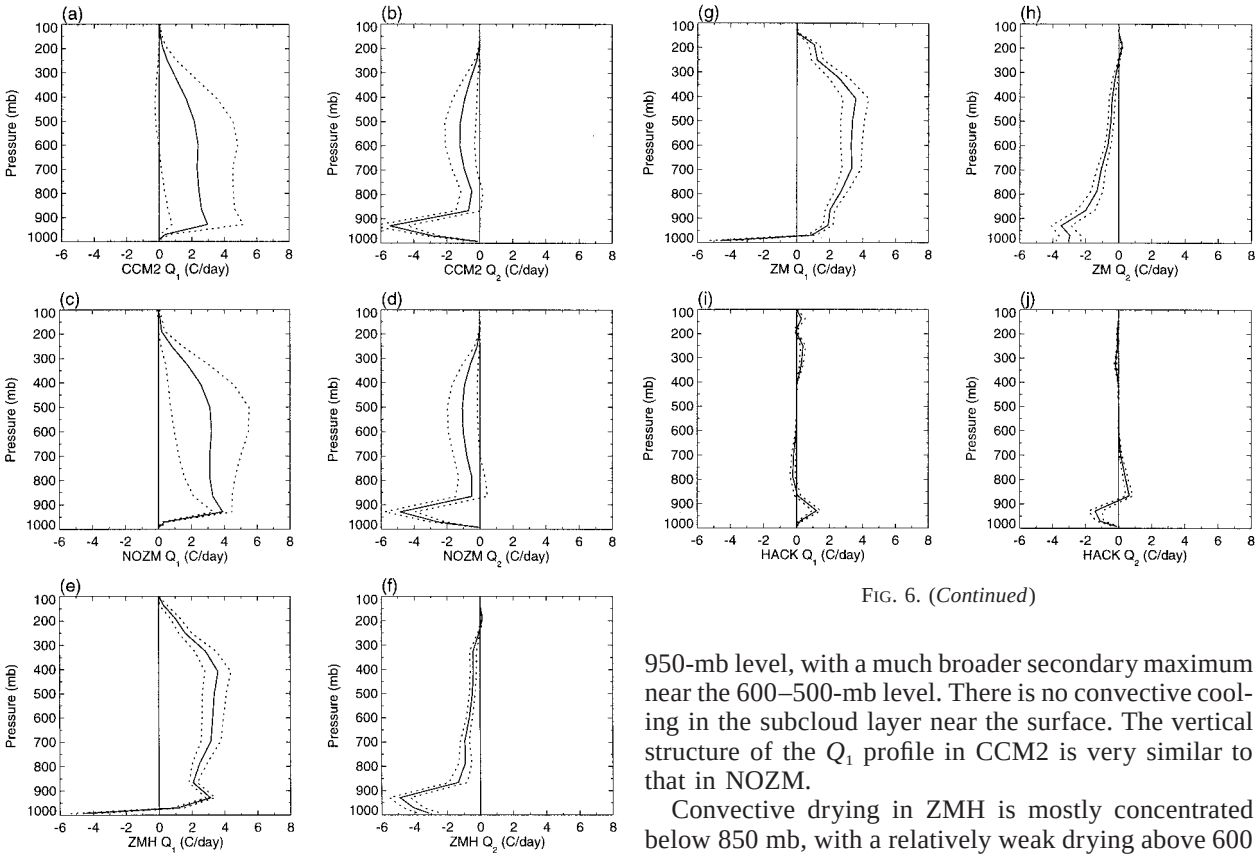

FIG. 6. Vertical profiles of the 90-day average convective heating Q_1–Q_R (left panel) and drying Q_2 (left panel) for (a), (b) CCM2, (c), (d) NOZM, and (e), (f) ZMH simulations averaged over the warm pool. In ZMH, the total convective heating and drying are further decomposed into the contributions from (g), (h) the ZM scheme and (i), (j) the Hack scheme. The dotted lines are one standard deviations from the average computed from the 90-daily value time series.

FIG. 6. (*Continued*)

penetrative plumes, whereas the Hack scheme describes convection as a layer-by-layer mixing process. As such, convection represented by the ZM scheme penetrates much deeper into the upper troposphere and the heating is more elevated than that from the Hack scheme. Figure 6 shows the vertical profiles of the mean convective heating Q_1–Q_R (for convenience, it will be referred to simply as Q_1 hereafter) and drying Q_2 averaged over the warm pool and the last 90 days of the 150-day simulations for CCM2 (Figs. 6a,b), NOZM (Figs. 6c,d), and ZMH (Figs. 6e,f). Also shown are the standard deviations from the averages (dotted lines), which measure the temporal variability of Q_1 and Q_2. In the case of the ZMH simulation, Q_1 and Q_2 are partitioned into the contributions from the ZM scheme (Figs. 6g,h) and the Hack scheme (Figs. 6i,j), respectively. The convective heating in ZMH reaches a maximum near the 400-mb level, with significant cooling associated with the convective downdrafts near the surface. A secondary maximum is located near 950 mb. In comparison, the maximum convective heating in NOZM is located at the 950-mb level, with a much broader secondary maximum near the 600–500-mb level. There is no convective cooling in the subcloud layer near the surface. The vertical structure of the Q_1 profile in CCM2 is very similar to that in NOZM.

Convective drying in ZMH is mostly concentrated below 850 mb, with a relatively weak drying above 600 mb and slight moistening near the 200-mb level. In the NOZM simulation, in addition to strong drying below 850 mb, there is a broad secondary maximum in the middle troposphere near 500–600 mb, about the same level as the secondary maximum heating. This is also qualitatively similar to the CCM2 profile (Fig. 6b). The partitioning between the ZM scheme and the Hack scheme shows that deep convection is dominant in the total convective heating over the warm pool and is almost entirely taken up by the ZM scheme. However, this is not to discount the importance of the Hack scheme in the CCM3 climate simulation. From Figs. 6i,j it is clear that the Hack scheme acts to produce shallow convection and possible upper-level convection in CCM3. The vertical structures of heating and drying below 700 mb—that is, heating and drying in the lower levels and cooling and moistening above—is characteristic of the nonprecipitating shallow convection. The relatively small magnitude of Q_1 and Q_2 from the Hack scheme is due to the fact that the warm pool is dominated by deep convection.

The vertical structures of the convective heating and drying in these short simulations exhibit many characteristics of the long-term average Q_1 and Q_2. Figure 7 shows the meridional-height cross section of the total convective heating and drying in the 5-yr CCM2 and CCM3 simulations presented in section 4. The partitioning between the heating generated by the Hack scheme and the ZM scheme in CCM3 is also shown.

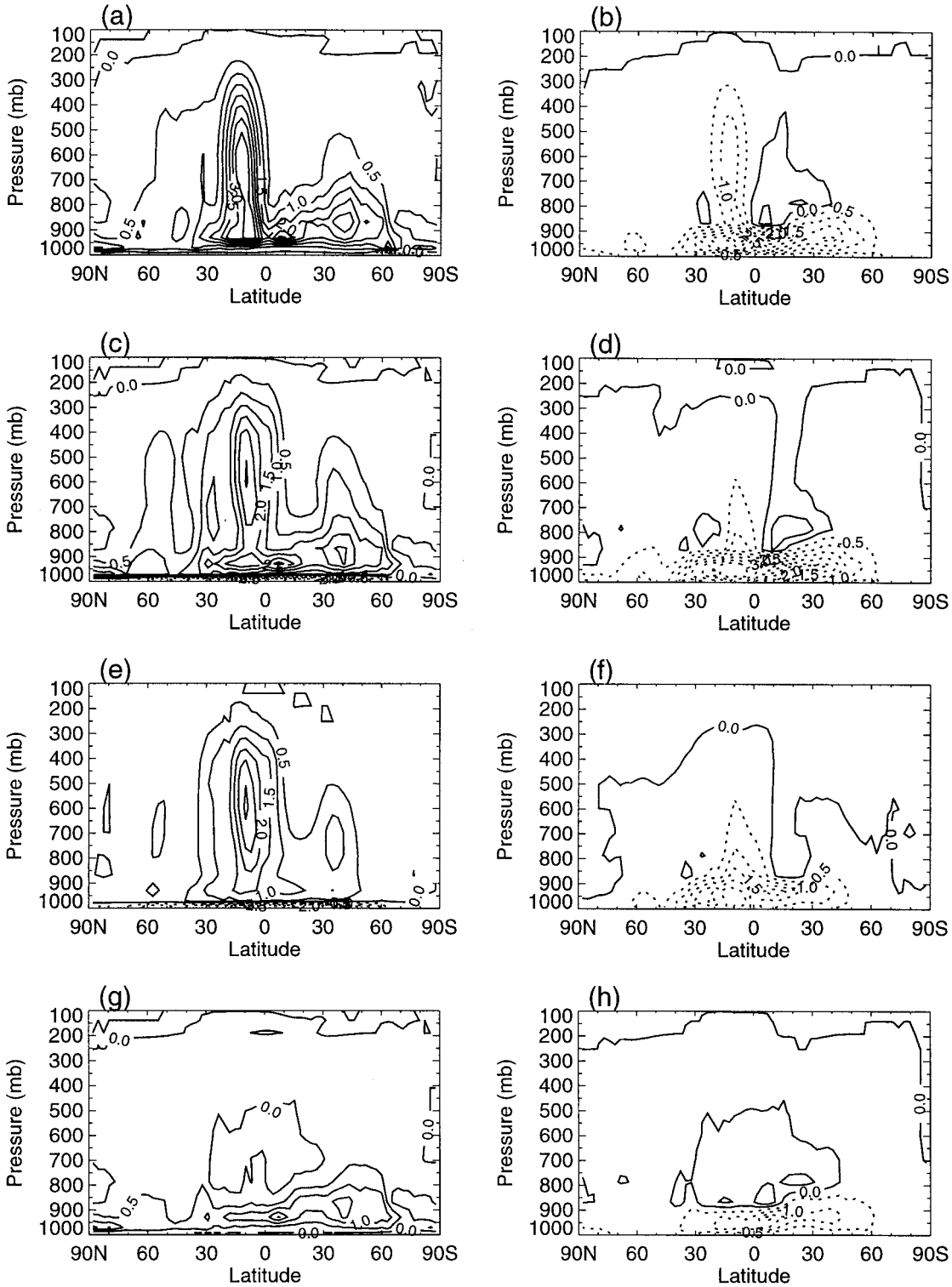

FIG. 7. Longitude–pressure cross sections (zonal mean) of total condensational heating and drying for CCM2 (a), (b) and CCM3 (c), (d). In the case of CCM3, the total convective heating and drying are partitioned into contributions from the ZM scheme (e), (f) and the Hack scheme (g), (h). Contour intervals are every 0.5°C day^{-1}.

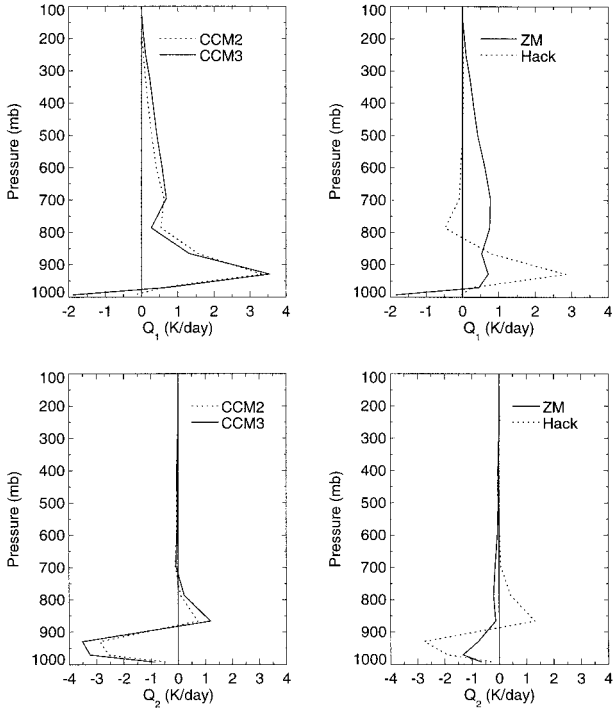

FIG. 8. The vertical profiles of Q_1 and Q_2 from CCM2 and CCM3 (left panel) and their partitioning into the contributions from the ZM scheme and the Hack scheme in CCM3 (right panel) averaged in the subtropical trade wind region of the central to eastern Pacific.

The three major diabetic heating zones in the rising branch of the Hadley cell and the midlatitude storm tracks are well simulated in both CCM2 and CCM3. However, similar to the short runs, a clear secondary maximum in convective drying in the middle tropical troposphere is observed in CCM2, but not in CCM3. In the case of CCM3, the partitioning between the Hack scheme and the ZM scheme shows the relative contribution of each to the total convective heating and drying. There is a broad maximum heating in the midtroposphere and significant cooling near the surface associated with convective downdraft from the ZM scheme. Although the total convective heating is dominated by the deep convection in the Tropics, shallow convection accounts for a significant part of the total heating in the subtropics and midlatitudes. As an example, Fig. 8 shows the Q_1 and Q_2 profiles from CCM2, CCM3, and its partitioning into the ZM scheme and the Hack scheme averaged over the trade wind regime of the central and eastern subtropical Pacific (from 10° to 30°N, and from 150° to 120°W). The net convective heating and drying in CCM3 are very similar to those in CCM2 except the cooling near the surface associated with the convective downdrafts in CCM3. Due to the suppressed conditions, the convective heating from the ZM scheme is generally small and is largely confined to the lower half of the troposphere. On the other hand, the Hack scheme is able to produce a significant amount of shallow convection, heating and drying the lower cloud layer below 900 mb and cooling and moistening the layers above. Clearly, in the climate regime that favors shallow convection, such as the subtropical trade wind regime, the Hack scheme becomes particularly important in producing shallow convection. Cumulus clouds from shallow convection can have a significant impact on the global radiation energy budget (Ramanathan et al. 1989).

The distribution of Q_1 and Q_2 in the warm pool can be compared with the observations from the recent Tropical Ocean Global Atmosphere Coupled Ocean–Atmosphere Response Experiment (TOGA COARE) field experiment in the western Pacific. Using rawinsonde data collected during TOGA COARE, Frank et al. (1996) computed Q_1 and Q_2 as the residual of the large-scale heat and moisture budgets. They found that the level of maximum Q_1 was located near 400 mb. This is qualitatively similar to the Q_1 distribution of the ZMH run. However, no significant cooling was found from the COARE observations, possibly due to the coarse vertical resolution of the soundings. The numerical simulation of a convection system in COARE by Wu and Moncrieff (1996) and the surface observations by Parsons et al. (1994) during COARE suggest that there is considerable convective cooling in the subcloud layer. The COARE-observed Q_2 has its maximum drying at the 800-mb level or higher depending on the area considered. In comparison, the levels of maximum drying in both ZMH and NOZM are lower. Examination of the time series and height cross sections of the COARE-observed Q_2 by Lin and Johnson (1996) indicates that the higher level of maximum Q_2 observed in COARE are associated with the stratiform precipitation. While the Q_2 distribution south of the equator during the COARE intensive observing period exhibits many stratiform precipitation characteristics, in the low-level convergence zone north of the equator where convection dominates, the observed Q_2 has a distinct maximum near the 850-mb level, in closer agreement with the level of maximum drying in the model simulations.

Figures 9 and 10 show the temperature and moisture time series averaged over the warm pool at 250, 500, and 1000 mb, respectively, for ZMH, NOZM, and CCM2. The differences between CCM2 and NOZM signify the effect of all the changes from CCM2 to CCM3 except the ZM convection scheme. In general, they are relatively small except for temperature at the 250-mb level, where the NOZM run is colder by 1°–2° in the later half of the simulation. Several factors may have contributed to the colder upper troposphere in the NOZM run. First, the model tunable parameters in CCM3 are adjusted for the standard CCM3 configuration. When the ZM scheme is removed, the top of the atmosphere will not be in energy balance, causing climate drift in long runs. Second, noting that deeper convection resulting from the use of the ZM scheme produces a moister upper troposphere, the critical relative

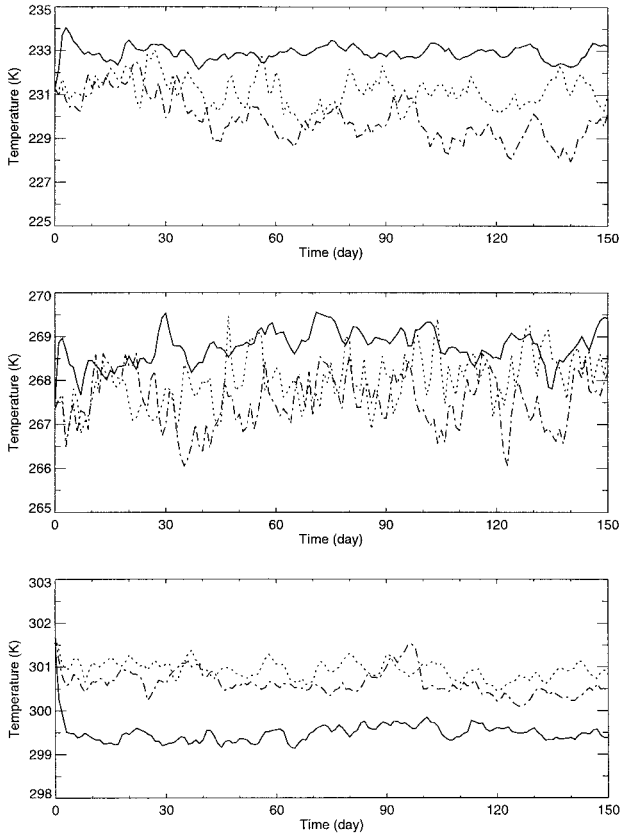

FIG. 9. Time series of temperature at (a) 250, (b) 500, and (c) 1000 mb for ZMH (solid line) and NOZM (dashed–dotted line) and CCM2 (dotted line).

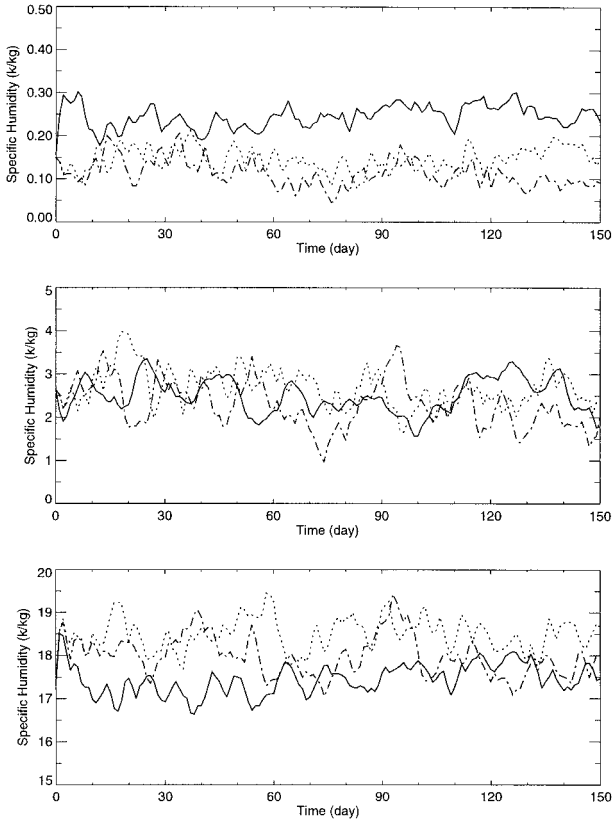

FIG. 10. Same as Fig. 9 but for moisture.

humidity for cloud formation in CCM3 is adjusted upward to produce a reasonable cloud amount. Therefore, when the ZM scheme is removed but the same critical relative humidity value is used in NOZM, less cloud is produced than in CCM2. This results in more loss in longwave radiation at the top of the atmosphere and more longwave cooling in the upper troposphere in NOZM.

ZMH simulation is systematically different from the other two runs. Use of the ZM scheme results in a warmer middle and upper troposphere and a colder surface/boundary layer. These changes are similar to those observed in the long-term simulations in section 4. Note that most of the temperature changes occur immediately after the initiation of the model simulation. As will be further discussed, these changes reflect the adjustment of the atmospheric thermodynamic state toward a quasi equilibrium with the atmospheric deep convection in the ZMH simulation.

The moisture field in the ZMH simulation is also increased to a level much higher than in NOZM and CCM2 in the upper troposphere. In the midtroposphere, the specific humidity in ZMH is comparable to that in the NOZM and CCM2 simulations, whereas in the lower troposphere, it decreases to lower values than those in NOZM and CCM2. This is a direct result of the more efficient transport of moisture from the lower troposphere to the upper troposphere by deep convection.

The role of the penetrative convection in reducing the surface latent heat flux and wind stress in CCM3 is demonstrated in Fig. 11, which shows the time series of surface latent heat flux and wind speed averaged over the warm pool for ZMH, NOZM, and CCM2. For the two runs without the penetrative convection—that is, NOZM and CCM2, surface latent heat flux and wind speed in the warm pool are very high and have similar characteristics in the temporal variations. On the other hand, in the ZMH simulation surface latent heat flux and wind speed are reduced significantly. The average value for the last 90 days of the 150-day integration is 4.7 m s^{-1} for wind speed and 123 W m^{-2} for latent heat flux in ZMH compared to 7.3 and 8.1 m s^{-1} for wind speed and 165 and 161 W m^{-2} for latent heat flux in NOZM and CCM2, respectively. Again, most of the changes occur within the first few days of the model simulation.

In the ZMH simulation, as in the standard CCM3, the ZM scheme and the Hack scheme are used together. How much does the interaction of the two schemes contribute to the simulation? As discussed before, shallow convection represented by the Hack scheme in the suppressed regimes accounts for a significant part of the

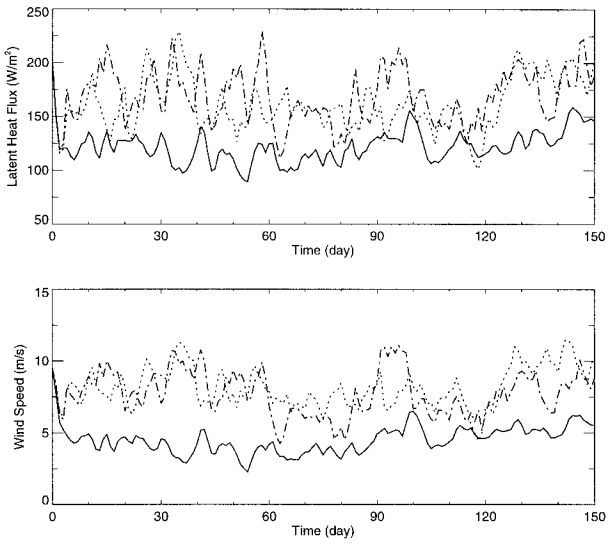

FIG. 11. Time series of (a) surface latent heat flux and (b) wind speed at the lowest model level (992 mb) averaged over the warm pool. Solid lines are for ZMH, dashed–dotted lines are for NOZM, and dotted lines are for CCM2.

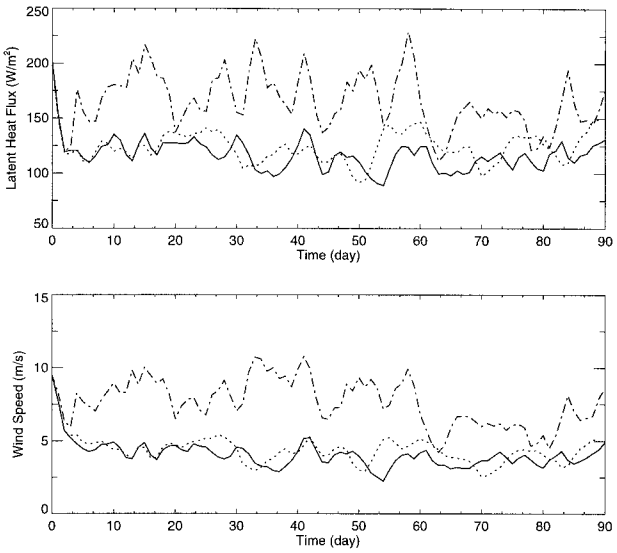

FIG. 12. Same as in Fig. 11 except the dotted line is from the experiment using the ZMH configuration without the Hack scheme.

total convective heating. Its contribution to the global radiation budget has an important impact on the global climate. On the other hand, the interaction of the two schemes in CCM3 is not expected to contribute significantly to the changes from NOZM to ZMH in the warm pool due to the dominance of deep convection there. To confirm this, we ran a 90-day simulation using the ZMH configuration but without the Hack scheme. Figure 12 plots the time series of the latent heat flux and surface wind speed averaged over the same warm pool area. The time series from NOZM and ZMH simulations are superposed for comparison. Indeed, the differences in the latent heat flux and wind speed between the ZMH simulation and the one without the Hack scheme are insignificant compared to the differences between the ZMH and NOZM simulations.

To summarize, the results averaged over the warm pool from the three 150-day simulations presented here demonstrate that representing convection by a deep penetrative scheme in CCM3 increases the temperature and moisture in the upper troposphere and decreases them in the lower troposphere. It also significantly reduces the surface latent heat flux and wind stress. These changes are similar to those observed from CCM2 to CCM3 in the long-term simulations.

Next, we attempt to explore the mechanisms of the interaction between convection and the large-scale fields that result in the effects of the deep convection as shown above. To this end, we follow the approach of Emanuel (1994) and Emanuel et al. (1994). In the tropical atmosphere, latent heat release through convection is largely balanced by the adiabatic cooling associated with the large-scale upward motion and radiative cooling, whereas the net heating to the atmosphere is a small difference of these large heating and cooling terms in the heat budget equation. Therefore, relating convection directly to the tropospheric temperature in a convecting atmosphere is appealing conceptually and can yield new insight into the interaction between convection and the large-scale circulation.

To demonstrate the link between convection and the tropospheric temperature, we make use of CAPE, which is defined as

$$\text{CAPE} = \int_{p_t}^{p_o} \left(\frac{1}{\rho_p} - \frac{1}{\rho_e}\right) dp, \tag{13}$$

where ρ_p and ρ_e are the density of the parcel to be lifted and that of the environmental air, respectively. Here p_o and p_t are the pressure at the parcel's originating level (normally the boundary layer or subcloud layer) and the level of neutral buoyancy (cloud top). CAPE is a measure of the kinetic energy a parcel would gain if lifted above the level of free convection. The time rate of change of CAPE is, after some manipulation following Emanuel et al. (1994),

$$\frac{\partial \text{CAPE}}{\partial t} = \int_{p_t}^{p_o} \left\{\left(\frac{\partial T}{\partial p}\right)_{\text{rm}} \frac{C_p \partial \theta_{\text{eb}}}{\theta_{\text{eb}} \partial t} + \frac{\partial}{\partial t}\left(\frac{\partial \phi}{\partial p}\right)\right\} dp, \tag{14}$$

where $\phi = gz$ is the geopotential, θ_{eb} is the equivalent potential temperature of the air parcel being lifted from the boundary layer, a conserved quantity following a reversible moist adiabat. Here, $(\partial T/\partial p)_{\text{rm}}$ is the temperature change with pressure following a reversible moist adiabat, or constant saturation entropy. Carrying out the integration in (14) with respect to p gives

$$\frac{\partial}{\partial t}(\phi_t - \phi_o) = (T_o - T_t)\frac{C_p \partial \theta_{\text{eb}}}{\theta_{\text{eb}} \partial t} - \frac{\partial \text{CAPE}}{\partial t}, \tag{15}$$

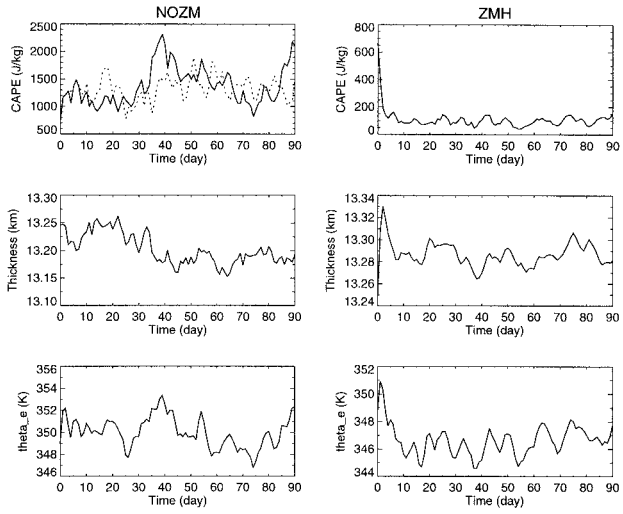

FIG. 13. Time series of CAPE (top panel), the tropospheric thickness (second panel), and the boundary layer θ_e (bottom panel). The left panel is for NOZM and the right panel is for ZMH. CAPE for CCM2 is superposed as the dotted line in the left panel.

where T_o and T_t are temperatures at p_o and p_t, respectively.

Arakawa and Schubert (1974) assume that the large-scale generation of the cloud work function (which is the same as CAPE in the special case of nonentraining plumes) and its consumption by convection are in *quasi equilibrium* on timescales of the order of days. In other words, the net change of the cloud work function with time is much smaller than the generation of it by the large-scale processes. If we neglect the last term on the right-hand side, (15) becomes

$$\frac{\partial}{\partial t}(\phi_t - \phi_o) \approx (T_o - T_t)\frac{C_p \partial \theta_{eb}}{\theta_{eb} \partial t}. \qquad (16)$$

It states that, when convection and the large-scale processes are in quasi equilibrium, changes of the thickness (mean virtual temperature) of the convecting layer are mainly determined by the changes in the equivalent potential temperature of the boundary layer air that rises into the cumulus clouds. In other words, under quasi equilibrium the effect of convection on the tropospheric temperature field is to ensure that convection always produces enough heating to restore the tropospheric temperature to a level dictated by the equivalent potential temperature of the subcloud layer air, which may be affected by convection as well. In such a case, the interaction between convection and the large-scale atmosphere may be easily understood and incorporated in analytical models of the tropical atmosphere. This approach has recently been pursued by Yu and Neelin (1997).

To examine to what extent the simulated tropical atmosphere exhibits quasi equilibrium characteristics and how it reaches quasi equilibrium, Fig. 13 shows the time series of the daily values of CAPE, the thickness of the troposphere $(\phi_t - \phi_O)/g$, and the boundary layer equivalent potential temperature averaged over the warm pool from the first 90 days of the NOZM and ZMH simulations. Here θ_e from the lowest model layer (992 mb) is used to represent the boundary layer value for the air rising into the cloud. Here p_o is taken to be the pressure at the third model level above the surface (929 mb), and p_t is taken to be the model level at 189 mb. The choice of a specific value for p_t is admittedly arbitrary. At a particular grid point, convection may not be always active, and the nonbuoyant level may not be at this particular level. However, on average over a convectively active region such as the warm pool, assuming the top of convection near 200 mb seems reasonable. Furthermore, this assumption does not affect our conclusions on whether the atmosphere exhibits a quasi-equilibrium behavior since quasi equilibrium, by definition, is measured by the relative magnitude of the temporal variation of CAPE, which is not affected by the choice of p_t in computing the thickness.

The CAPE in ZMH changes insignificantly with time except at the beginning of the integration, where it decreases from the initial value of close to 700 J kg^{-1} to less than 200 J kg^{-1} in a few days. Comparing to the magnitude of CAPE generation by the radiative cooling or large-scale adiabatic ascent on the order of 1000 J kg^{-1} day^{-1} (Emanuel 1994), it is clear that the large-scale processes and convection in ZMH are in quasi-equilibrium after the first few days of the model integration. In contrast, CAPE in NOZM and CCM2 starts with a similar initial value to that in ZMH, but increases to much larger values (on the order of 1000–1500 J kg^{-1}). The temporal variability of CAPE in NOZM is very large (an order of magnitude larger than in ZMH), varying from about 700 J kg^{-1} to more than 2000 J kg^{-1}, an indication that the atmosphere is not in a quasi-equilibrium state. The large CAPE values in NOZM and CCM2 implies that the atmosphere is much less stable than in the ZMH run. The difference in CAPE between NOZM/CCM2 and ZMH is qualitatively similar to that in the 5-yr mean between CCM2 and CCM3 in Truk Island given in section 4.

The large CAPE value and its variation in NOZM/CCM2 are caused by the inefficiency of the convection scheme used in these simulations to transport heat and moisture effectively to the upper troposphere. It should be noted that the Hack scheme is a three-layer moist convective adjustment scheme in mass flux form. Thus, by design it removes only instability locally without reference to the column instability. On the other hand, CAPE, as defined in (13), measures the overall convective instability of a tropospheric column. When the Hack scheme is used, the local stability of an atmospheric column is checked layer by layer, starting from the top of the boundary layer. If the air in the adjacent two layers is found to be convectively unstable, moist adjustment is applied. For a typical tropospheric moist static energy profile with both the moist static energy

and its saturation value reaching a minimum in the midtroposphere and increasing above, this procedure will remove convective instability in the lower troposphere. However, in the upper-tropical troposphere the Hack scheme will not produce convection to transport heat and moisture further upward, although the atmospheric column as a whole may still be unstable with respect to the boundary layer air. Thus, CAPE can be significant after the application of the Hack scheme. This does not mean that the Hack scheme cannot produce convection in the upper troposphere at all. While the upper troposphere on average is moist statically stable, at a given time step in the model, due to the radiative cooling or large-scale advection some layers can become unstable locally. In such locally unstable layers, the Hack scheme will be activated to mix these layers, resulting in convective heating and drying. Because convection in the Hack scheme is determined by the local instability, the temporal fluctuation of CAPE can be significant.

The quasi-equilibrium assumption is well supported by the observations. Using the 12-hourly soundings from east and south Asia, Arakawa and Chen (1987) showed that the surface relative humidity and the temperature lapse rate normalized about the surface moist adiabatic value are negatively correlated, clustering around the constant cloud work function curves for both the spatial and temporal variations. Recently, Brown and Bretherton (1997) examined the strict quasi-equilibrium approximation (i.e., $\partial \text{CAPE}/\partial t = 0$) on timescales of a month and longer, and on space scales of several hundred kilometers and larger in the tropical oceans. Using 11 yr of the microwave sounding unit temperature data and COADS surface data, they found that while the correlations between the perturbations of the mean tropospheric temperature and those of the boundary layer equivalent potential temperature are positive on all scales considered, they are considerably weaker than expected from the strict quasi-equilibrium approximation. However, when only the observations with precipitation rates greater than 196 mm month^{-1} ($\sim$6.5 mm day^{-1}) are considered so that there is sufficient convective activity to communicate the changes of the equivalent potential temperature in the subcloud layer to the troposphere, the correlation is significantly improved, particularly over the western Pacific warm pool. Therefore, they suggest that the strict quasi-equilibrium assumption is qualitatively correct for long time- and space scales with precipitation greater than 196 mm month^{-1}. Examination of the TOGA COARE data on timescales of several days also suggests that the atmosphere exhibits a large degree of quasi equilibrium (Brown 1994; Stevens et al. 1997).

Within the framework of the quasi equilibrium, the temperature changes from NOZM to ZMH as seen in Fig. 9 can be easily understood. At the beginning of the ZMH run, convective stabilization and large-scale destabilization are not in quasi equilibrium, and the amount of CAPE in the atmosphere is larger than what is required by the equilibrium state. Thus, reaching equilibrium requires $\partial \text{CAPE}/\partial t < 0$. From (15), this means an increase in the thickness of the troposphere in addition to that corresponding to the change of the subcloud layer equivalent potential temperature. The large increase in the thickness of the atmosphere compared to the change of the boundary layer equivalent potential temperature at the beginning of the model integration clearly reflects this stabilization process (Fig. 13). Accompanying this thickness increase, the temperature in the middle and upper troposphere increases by several degrees in a short time period (Fig. 9). The CAPE decrease is accomplished through both warming in the middle and upper troposphere and cooling and drying in the subcloud layer. After the first few days of the adjustment, the large-scale atmosphere and convection reach a quasi equilibrium. Under this quasi equilibrium state, the atmosphere in ZMH is warmer compared to that in NOZM.

The large-scale circulation also undergoes a significant change during the adjustment to quasi equilibrium (Fig. 11). This change can be understood with the argument of Neelin and Held (1987), who showed that the large-scale low-level mass convergence is largely governed by the effective static stability of the atmosphere. A weak low-level convergence and circulation will result when the atmosphere is more moist statically stable, and vice versa. As we have shown (Figs. 4, 9, and 10), when the ZM scheme is included in the simulations, the atmosphere is warmer and more moist in the upper troposphere, and relatively cold and dry in the lower troposphere and the surface, both contributing to a more stable tropical troposphere. Correspondingly, based on Neelin and Held's argument the circulation should be weaker, resulting in a weaker surface flow and hydrological cycle. This is indeed the case, as can be seen from Fig. 11. The surface latent heat flux and the surface wind speed for the simulations with and without the ZM scheme start to diverge a few days after the initiation of the integration to respond to the changing thermal structure. The values of the latent heat flux and wind speed become systematically lower in ZMH than in NOZM and CCM2 after the atmosphere in ZMH reaches a more stable state, in agreement with the theory of Neelin and Held (1987).

To synthesize the interaction process, representation of deep convection in the CCM3 model produces a more stable troposphere as a result of the quasi-equilibrium adjustment between convection and the large-scale atmosphere. This is achieved through convective heating and moistening in the upper and middle troposphere and cooling and drying in the lower troposphere and surface. The coupling between the atmospheric dynamic and thermodynamic structures (Neelin and Held 1987) leads to a weak atmospheric circulation, resulting in low surface evaporation and surface wind stress.

It should be pointed out here that while the quasi-equilibrium concept is a very useful tool for understand-

ing the interaction between convection and the large-scale circulation, it has some serious weaknesses when applying it to climate studies. One fundamental weakness is that the moisture field in the troposphere above the boundary layer is not considered except through its effect on the virtual temperature. As discussed in section 4, water vapor is an important climate parameter, and it has a significant impact on the global climate change. Thus, lack of more active consideration of the moisture transport in the quasi-equilibrium concept may limit its application to the climate change. Second, quasi equilibrium cannot predict the amount of CAPE in the atmosphere. Therefore, for climate change, CAPE may not be estimated accurately (Yi et al. 1998). Nevertheless, the quasi-equilibrium concept casts a framework that makes understanding the interaction of convection and the large-scale much easier.

As discussed in section 4, some of the systematic biases in the simulated thermal structure in CCM3 are probably related to the ZM convection scheme. The main weakness of the scheme is that it produces some excessive drying in the lower to middle troposphere. The CCM3 simulation of the intraseasonal variation of the atmosphere has also been known to exhibit some weakness of the model. Due to the close association of convective activity and the intraseasonal oscillations, the ZM scheme may also be responsible for part of the model weakness in this aspect. More studies are needed to improve it.

6. Concluding remarks

This study examines the response of the climate simulation by the NCAR CCM3 to the (Zhang and McFarlane 1995) convection scheme. It is shown that the CCM3 simulation is significantly improved in the precipitation, surface evaporation, and surface wind stress in the tropical convective regimes, particularly in the western Pacific warm pool. However, the thermodynamic structures, especially the water vapor field, in the tropical free troposphere is degenerated compared to the CCM2 simulation. Some possible reasons for it are discussed.

To investigate the role of the Zhang and McFarlane convection scheme in the improvement of the climate simulation and to understand the mechanism of the convection and large-scale interaction, the results over the warm pool from three 150-day-long simulations with and without the Zhang and McFarlane scheme were examined. It is shown that many features of the differences between the CCM3 and CCM2 simulations are observed in the two short runs using the CCM3 configuration—one with the ZM convection scheme (ZMH) and the other without the ZM convection scheme (NOZM). These include the vertical convective heating distribution, temperature and moisture structure, suface winds, and evaporation. These results suggest that the ZM convection scheme makes a significant contribution to the improvement of the simulated climate in CCM3. Other model changes from CCM2 to CCM3 also affected the model simulation in the Pacific warm pool, particularly the upper-tropospheric temperature.

One important difference between the Zhang and McFarlane scheme and the Hack scheme in representing convection is that the former considers convection as consisting of deep penetrative plumes and the latter treats convection as a layer-by-layer mixing process. Related to this difference is the use of the different closure assumptions. In the Zhang and McFarlane scheme convection is determined by the amount of CAPE in an atmospheric column, whereas in the Hack scheme convection is dictated by the local instability of a layer. As a result, the interaction between convection and the large-scale circulation is significantly different using the two schemes. The simulated atmosphere using the Zhang and McFarlane scheme is in quasi equilibrium with convection. One consequence of such a quasi equilibrium is that the mean tropospheric temperature is largely determined by the boundary layer equivalent potential temperature. On the other hand, no such equilibrium is found in the simulation using the Hack scheme, which produces large temporal variability as well as magnitude in CAPE.

Under the quasi-equilibrium framework, it is shown that the transition from the less stable atmosphere corresponding to the Hack scheme to the more stable atmosphere characteristic of the CCM3 simulation takes place at the beginning of the time integration when the atmosphere adjusts itself toward the quasi equilibrium with convection. Deep convection, as represented by the Zhang and McFarlane scheme, produces a more stable atmosphere compared to that of the Hack scheme. Since the atmospheric stratification strongly affects the low-level mass convergence in the Tropics, in response to such an atmospheric stratification, the tropical atmospheric circulation is weaker (Neelin and Held 1987; Zhang 1994), resulting in lower surface winds and smaller surface evaporation, particularly in the western Pacific warm pool.

Acknowledgments. This research was supported by the Environmental Science Division of U.S. Department of Energy under Grants DEFG 0391 ER 61198 (GJZ) and DE-AI05-92ER61376 (JTK) as part of the Atmospheric Radiation Measurement Program, and by NSF under Grants ATM95-25800 (GJZ) and ATM94-05024 (JTK, PJR). The authors would like to thank Jim Hack for his help in the process of implementing the ZM convection scheme in CCM3. GJZ acknowledges the help from Jim Rosinski at various stages in the course of this work. He also thanks V. Ramanathan for his encouragement and for his interest in this work. The reviewers are thanked for their helpful comments. The FSU wind stress data are obtained from the NCAR archive maintained by the NCAR Scientific Computing Division.

REFERENCES

Arakawa, A., and W. H. Schubert, 1974: Interaction of a cumulus cloud ensemble with the large-scale environment. Part I. *J. Atmos. Sci.*, **31,** 674–701.

——, and J.-M. Chen, 1987: Closure assumptions in the cumulus parameterization problem. *Short- and Medium-Range Numerical Weather Prediction,* T. Matsumo, Ed., J. Meteor. Soc. Japan, 107–131.

Bonan, G. B., 1996: A land surface model (LSM version 1.0) for ecological, hydrological and atmospheric studies: Technical description and user's guide. NCAR Tech. Note NCAR/TN-417+STR, 150 pp. [Available from National Center for Atmospheric Research, Boulder, CO 80307.]

Brown, R. G., 1994: A modeling and observational study of convective interaction with large-scale dynamics in the Tropics. Ph.D. dissertation, University of Washington, 193 pp. [Available from Dept. of Atmospheric Sciences, University of Washington, Seattle, WA 98195.]

——, and C. S. Bretherton, 1997: A test of the strict quasi-equilibrium theory on long space and timescales. *J. Atmos. Sci.,* **54,** 624–638.

Emanuel, K. A., 1994: *Atmospheric Convection.* Oxford University Press, 580 pp.

——, J. D. Neelin, and C. S. Bretherton, 1994: On large-scale circulations in convecting atmospheres. *Quart. J. Roy. Meteor. Soc.,* **20,** 1111–1143.

Frank, W. M., H. Wang, and J. L. McBride, 1996: Rawinsonde budget analyses during the TOGA COARE IOP. *J. Atmos. Sci.,* **53,** 1761–1780.

Gates, W. L., 1992: AMIP: The atmospheric model intercomparison project. *Bull. Amer. Meteor. Soc.,* **73,** 1962–1970.

Hack, J. J., 1994: Parameterization of moist convection in the National Center for Atmospheric Research community climate model (CCM2). *J. Geophys. Res.,* **99,** 5551–5568.

——, B. A. Boville, B. P. Briegleb, J. T. Kiehl, P. J. Rasch, and D. L. Williamson, 1993: Description of the NCAR Community Climate Model (CCM2). NCAR Tech. Note NCAR/TN-382+STR, 108 pp. [Available from National Center for Atmospheric Research, Boulder, CO 80307.]

——, ——, J. T. Kiehl, P. J. Rasch, and D. L. Williamson, 1994: Climate statistics from the National Center for Atmospheric Research Community Climate Model CCM2. *J. Geophys. Res.,* **99,** 20 785–20 813.

——, J. T. Kiehl, and J. W. Hurrell, 1998: The hydrologic and thermodynamic characteristics of the NCAR CCM3. *J. Climate,* **11,** 1179–1206.

Hurrell, J. W., J. J. Hack, and D. P. Baumhefner, 1993: Comparison of NCAR Community Climate Model climates. NCAR Tech. Note NCAR/TN-395+STR, 335 pp. [Available from National Center for Atmospheric Research, Boulder, CO 80307.]

——, ——, B. A. Boville, D. L. Williamson, and J. T. Kiehl, 1998: The dynamical simulation of the NCAR Community Climate Model version 3 (CCM3). *J. Climate,* **11,** 1207–1236.

Kiehl, J. T., 1994: Sensitivity of a GCM climate simulation to differences in continental versus maritime cloud drop size. *J. Geophys. Res.,* **99,** 23 107–23 115.

——, and B. P. Briegleb, 1992: Comparison of the observed and calculated clear sky greenhouse effect—Implications for climate studies. *J. Geophys. Res.,* **97,** 10 037–10 049.

——, J. J. Hack, and B. P. Briegleb, 1994: The simulated earth radiation budget of the National Center for Atmospheric Research Community Climate Model CCM2 and comparisons with the Earth Radiation Budget Experiment (ERBE). *J. Geophys. Res.,* **99,** 20 815–20 827.

——, ——, M. H. Zhang, and R. D. Cess, 1995: Sensitivity of a GCM climate to enhanced shortwave cloud absorption. *J. Climate,* **8,** 2200–2212.

——, ——, G. B. Bonan, B. A. Boville, B. P. Briegleb, D. L. Williamson, and P. J. Rasch, 1996: Description of the NCAR Community Climate Model (CCM3). NCAR Tech. Note NCAR/TN-420+STR, 152 pp. [Available from National Center for Atmospheric Research, Boulder, CO 80307.]

——, ——, ——, ——, D. L. Williamson, and P. J. Rasch, 1998a: The National Center for Atmospheric Research Community Climate Model: CCM3. *J. Climate,* **11,** 1131–1150.

——, ——, and J. W. Hurrell, 1998b: The energy budget of the NCAR Community Climate Model: CCM3. *J. Climate,* **11,** 1151–1178.

Legates, D. R., and C. J. Willmott, 1990: Mean seasonal and spatial variability in gauge corrected precipitation. *Int. J. Climatol.,* **10,** 111–127.

Lin, X., and R. H. Johnson, 1996: Heating, moistening, and rainfall over the western Pacific warm pool during TOGA COARE. *J. Atmos. Sci.,* **53,** 3367–3383.

Neelin, J. D., and I. M. Held, 1987: Modeling tropical convergence based on the moist static energy budget. *Mon. Wea. Rev.,* **115,** 3–12.

Oberhuber, J. M., 1988: An atlas based on the ''COADS'' data set: The budgets of heat, buoyancy and turbulent kinetic energy at the surface of the global ocean. Max Planck Institute for Meteorology Rep. 15, 199 pp. [Available from Max-Planck-Institut für Meteorologie, Bundesstr. 55, D-20146 Germany.]

Parsons, D., and Coauthors, 1994: The integrated sounding systems: Description and preliminary observations from TOGA COARE. *Bull. Amer. Meteor. Soc.,* **75,** 553–567.

Ramanathan, V., R. D. Cess, E. F. Harrison, P. Minnis, B. P. Barkstrom, E. Ahmad, and D. L. Hartmann, 1989: Cloud radiative forcing and climate: Results from the Earth Radiation Budget Experiment. *Science,* **243,** 57–63.

——, B. Subasilar, G. J. Zhang, W. Conant, R. D. Cess, J. T. Kiehl, H. Grassl, and L. Shi, 1995: Warm pool heat budget and shortwave cloud forcing: A missing physics? *Science,* **267,** 499–503.

Smull, B. F., and M. J. McPhaden, 1996: Comparison of NCEP/NCAR reanalyzed fields and surface observations over the TOGA-TAO array. *Proc. 21st Climate Diagnostics and Prediction Workshop,* Huntsville, AB, 57–60.

Stevens, B., D. A. Randall, X. Lin, and M. T. Montgomery, 1997: Comments on ''On large-scale circulation in convecting atmospheres'' by Kerry A. Emanuel, J. David Neelin, and Christopher S. Bretherton. *Quart. J. Roy. Meteor. Soc.,* **123,** 1771–1778.

Williamson, D. L., J. Olson, and B. A. Boville, 1998: A comparison of semi-Lagrangian and Eulerian tropical climate simulations. *Mon. Wea. Rev.,* **126,** 1001–1012.

Wu, X. Q., and M. W. Moncrieff, 1996: Collective effects of organized convection and their approximation in general circulation models. *J. Atmos. Sci.,* **53,** 1477–1495.

Xu, K.-M., and K. A. Emanuel, 1989: Is the tropical atmosphere conditionally unstable? *Mon. Wea. Rev.,* **117,** 1471–1479.

Yi, B., A. Del Genio, and K. Lo, 1998: CAPE variations in the current climate and in a climate change. *J. Climate,* in press.

Yu, J. Y., and J. D. Neelin, 1997: Analytic approximations for moist convectively adjusted regions. *J. Atmos. Sci.,* **54,** 1054–1063.

Zhang, G. J., 1994: Effects of cumulus convection on the simulated monsoon circulation in a general circulation model. *Mon. Wea. Rev.,* **122,** 2022–2038.

——, and N. A. McFarlane, 1995: Sensitivity of climate simulations to the parameterization of cumulus convection in the Canadian Climate Centre general circulation model. *Atmos.–Ocean,* **33,** 407–446.

——, and M. J. McPhaden, 1995: The relationship between sea surface temperature and latent heat flux in the equatorial Pacific. *J. Climate,* **8,** 589–605.

——, and R. L. Grossman, 1996: Surface evaporation during the Central Equatorial Pacific Experiment: A climate-scale perspective. *J. Climate,* **9,** 2522–2537.

Zhang, M. H., 1996: Impact of the convection-wind-evaporation feedback on surface climate simulation in general circulation models. *Climate Dyn.,* **12,** 299–312.